

Heisenberg spins on an anisotropic triangular lattice: PdCrO₂ under uniaxial stress

Dan Sun,^{1,2} Dmitry A. Sokolov,¹ Richard Waite,^{3,4} Seunghyun Khim,¹ Pascal Manuel,⁴
Fabio Orlandi,⁴ Dmitry D. Khalyavin,⁴ Andrew P. Mackenzie,^{1,5} and Clifford W. Hicks^{1,6}

¹Max Planck Institute for Chemical Physics of Solids, Nöthnitzer Str. 40, 01187 Dresden, Germany

²Stewart Blusson Quantum Matter Institute, the University of British Columbia, Vancouver, V6T 1Z4 Canada

³H. H. Wills Physics Laboratory, University of Bristol, Bristol, BS8 1TL, United Kingdom

⁴ISIS Facility, Rutherford Appleton Laboratory, Chilton, Didcot, OX11 0QX, United Kingdom

⁵Scottish Universities Physics Alliance (SUPA), School of Physics and Astronomy,
University of St. Andrews, St. Andrews KY16 9SS, United Kingdom

⁶School of Physics and Astronomy, University of Birmingham, Birmingham B15 2TT, United Kingdom

(Dated: December 21, 2021)

When Heisenberg spins interact antiferromagnetically on a triangular lattice and nearest-neighbor interactions dominate, the ground state is 120° antiferromagnetism. In this work, we probe the response of this state to lifting the triangular symmetry, through investigation of the triangular antiferromagnet PdCrO₂ under uniaxial stress by neutron diffraction and resistivity measurements. The periodicity of the magnetic order is found to change rapidly with applied stress; the rate of change indicates that the magnetic anisotropy is roughly forty times the stress-induced bond length anisotropy. At low stress, the incommensuration period becomes extremely long, on the order of 1000 lattice spacings; no locking of the magnetism to commensurate periodicity is detected. Separately, the magnetic structure is found to undergo a first-order transition at a compressive stress of ~0.4 GPa, at which the interlayer ordering switches from a double- to a single- q structure.

Antiferromagnetic interactions are frustrated on a triangular lattice. When the spins are Heisenberg spins and nearest-neighbour interactions dominate, balancing interactions across the three bond directions leads to 120° order, in which the spin orientation rotates by $2\pi/3$ from site to site [1, 2]. Lifting the triangular symmetry may cause the magnetism to become incommensurate [3, 4]. However, propagation vectors tend to lock to commensurate values, because for commensurate orders the spins can find a single optimum configuration, while for incommensurate orders the state energy must be averaged over a 2π rotation of the spin orientation. A symmetry-breaking field may therefore need to exceed a threshold strength for the magnetism to become incommensurate. Such “lock-in” to commensurate periodicities has been observed in several non-triangular systems, such as, for example, CaFe₄As₃ [5, 6], Ba(Fe_{1-x}Co_x)₂As₂ [7], and lightly-doped Cr [8]; in all of these cases, the transition between commensurate and incommensurate states is first-order.

Independently of this potential commensurate-to-incommensurate transition, the possibility of tuning a triangular lattice through uniaxial stress has been considered before, and there are two possible directions, illustrated in Fig. 1(a) [3, 4, 9, 10]. By applying stress along a $\langle\bar{1}10\rangle$ direction, the atomic positions are pushed towards a square lattice, and the magnetic interactions may similarly evolve towards a square lattice with weak diagonal bonds. Alternatively, by applying stress along a $\langle 100\rangle$ direction, the atomic positions are pushed in the direction of 1D chains.

Here, we study the triangular antiferromagnet PdCrO₂ under tunable uniaxial stress applied along the $[\bar{1}10]$ lat-

tice direction. We will show that the magnetic interactions, like the atomic positions, evolve towards those of a square lattice. In other words, the interaction energy increases as bond length is reduced, which is intuitive. In this compound, insulating CrO₂ layers are separated by highly conducting Pd sheets. The Cr configuration is $3d^3$, and due to strong Hund’s coupling the three electron spins align to form robust $S = 3/2$ moments; the CrO₂ layers are Mott insulating [11–13]. Coupling between the Cr and Pd layers means that the magnetic structure in the Cr layers affects electronic transport properties. A downturn in resistivity shows that short-range correlation between Cr spins appears starting at around room temperature [14–16]. By ~100 K the correlation length becomes long enough to measurably influence the Hall and Nernst effects [17], and to yield substantial magnon drag in the thermopower [18]. By 40 K the in-plane correlation area reaches ~1000 sites, without interlayer correlation [19, 20]. Then, at $T_N = 37.5$ K, the layers lock together in a transition that appears to be first-order, and the order becomes long-range correlated in three dimensions [19].

The magnetic order spontaneously lifts the three-fold rotational symmetry of the non-magnetic lattice [16, 21]. The delafossite structure is rhombohedral: Cr sites in each layer are equidistant from three Cr sites in adjacent layers, so interlayer interactions balance and the layers cannot couple [23]. The rotational symmetry breaking provides a preferred orientation that allows coupling; the related delafossite compound CuCrO₂ also shows this rotational symmetry breaking [24, 25]. The spin plane for PdCrO₂ and CuCrO₂ contains the c axis, and the azimuthal angle takes one of three symmetrically equivalent

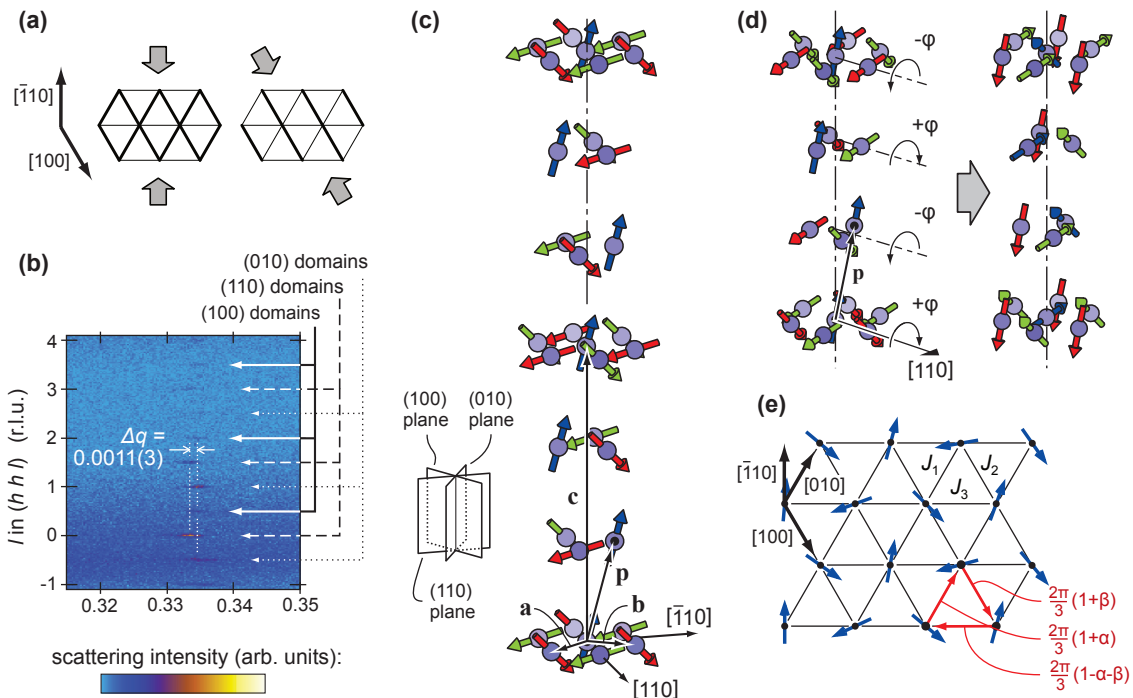


FIG. 1. (a) Conceptual illustration of a triangular lattice under in-plane uniaxial stress. Heavy lines denote shorter bonds, and potentially stronger magnetic interaction. Depending on the direction of the applied stress, the lattice can be pushed towards either a square lattice (left) or one-dimensional chains (right). (b) Neutron scattering intensity in unstressed PdCrO_2 , from Ref. [21]. As indicated, there are three domain types, that yield three sets of reflections. The offset Δq is explained in the text. (c) A magnetic structure of PdCrO_2 consistent with the magnetic scattering intensities reported in Ref. [22]. The circles are the Cr sites, and the illustrated structure is from a (110) domain. **a**, **b**, and **c** are the unit cell vectors of the nonmagnetic lattice. **p** is the vector that connects interlayer nearest-neighbor sites and lies within the spin plane; spins joined by **p** have the same colour. (d) Illustration of a collective spin rotation that does not alter any magnetic scattering intensities. Here, $\varphi = 60^\circ$. (e) An illustration of incommensurate order on a near-triangular lattice. The red text indicates the spin rotation angle along the indicated bond directions, and J_1 , J_2 , and J_3 are the nearest-neighbour magnetic interaction energies along the three bond directions.

possible orientations [21, 22].

We report results of neutron scattering and electrical resistivity measurements. The neutron diffraction data show that the rate of change of the magnetic structure with applied stress is large: the magnetic anisotropy is roughly forty times the stress-induced bond length anisotropy. The neutron data also reveal a stress-driven first-order transition in the interlayer ordering, which shows that the interlayer ordering probably reflects a delicate balance of interactions. This transition is apparent in the resistivity data. The resistivity data also reveal structure in the transition at T_N , which encourage further experimentation.

BACKGROUND

We begin with a description of the magnetic structure of PdCrO_2 as it is currently understood. Shown in Fig. 1(b) is neutron scattering data from nominally unstressed PdCrO_2 , reported in Ref. [21]. As indicated in

the figure, there are three sets of reflections, originating from three domain types, which we label by their spin plane. In Fig. 1(c), we illustrate a coplanar magnetic structure that gives a good fit to the scattering intensities reported in Ref. [22]. An anomalous Hall effect has been interpreted as evidence for a non-coplanar magnetic structure [26], and an observation of nonreciprocal transport could indicate that inversion symmetry is broken [27]. However, the quality of the fit of the coplanar structure in Fig. 1(c) is very good [21]. The Hall effect might be influenced by magnetic breakdown [28].

In the structure illustrated in Fig. 1(c), the spin plane is the (110) plane. The (100) and (010) planes are symmetrically equivalent, resulting in the three domain types. To understand the magnetic structure, it is useful to define a vector **p**, that connects interlayer nearest-neighbour sites and lies within the spin plane. Between spins that are connected by **p**, the components of the spins that are parallel to **p** are aligned ferromagnetically, and those perpendicular to **p** are aligned antiferromagnetically. This combination of ferromagnetic and anti-

ferromagnetic alignment means that the helicity alternates from layer to layer. It means that neutron reflections from a single domain are spaced along the l axis by $\Delta l = \frac{3}{2}$ r.l.u. (defined using a three-layer unit cell), rather than the $\Delta l = 3$ that would be obtained for a fully ferromagnetic or antiferromagnetic interlayer ordering. For $h = k = \frac{1}{3}$, (110) domains give reflections at $l = \frac{3}{2}n$, (100) domains at $\frac{1}{2} + \frac{3}{2}n$, and (010) domains at $1 + \frac{3}{2}n$, where n is an integer [21].

In Fig. 1(d) we illustrate a degree of freedom that is unconstrained by data so far: rotation of spins in alternating planes by angles $+\phi$ and $-\phi$ does not alter any neutron scattering intensities, for any value of ϕ . Incommensuration can therefore emerge as a spatial gradient in ϕ . In Fig. 1(e) we illustrate a generic construction of incommensurate order on a triangular lattice. If the spin rotation angle upon translation from site to site along the [010] direction is $\frac{2\pi}{3}(1 + \alpha)$, and that along [100] $\frac{2\pi}{3}(1 + \beta)$, then to linear order in α and β the reflection at $[h, k, l] = [\frac{1}{3}, \frac{1}{3}, l]$ moves to $[\frac{1}{3}(1 + \alpha), \frac{1}{3}(1 + \beta), l]$. In the illustration, the nearest-neighbor interaction strengths are $J_1 > J_2 > J_3$, which yields $\alpha > 0$ and $\alpha + \beta > 0$.

RESULTS: NEUTRON SCATTERING

A sample of cross section 1.37×0.21 mm² was mounted into piezoelectric-based uniaxial stress apparatus adapted for use in neutron scattering and muon spin rotation measurements, described in Ref. [29]. The central, exposed portion of the sample was 1.3 mm in length. The end portions of the sample were embedded in epoxy for transmission of force to the sample. These portions were screened from the neutron beam with cadmium foil. Growth of single crystals of PdCrO₂ more than 1–2 mm in extent remains a challenge, and there were voids in the sample that will have introduced stress inhomogeneity.

Measurements were performed using the WISH diffractometer at the ISIS Pulsed Neutron and Muon Source [30]. Compressive stress was applied along the [110] direction. Strain gauges were affixed to the sample holder to measure the applied stress, and the cell incorporates a mechanism for finding the zero-stress reading. We estimate an error of ± 3 MPa on this zero-stress reading. The largest compressive stress we applied was $\sigma_m = -0.40 \pm 0.08$ GPa. (Negative values denote compression.) Measurements were performed at 10 K, and temperature was kept constant, without thermal cycling, during changes in the applied force. In analysis of the neutron data, we index the reflections at all strains to the Bragg peaks at the smallest stress applied, $0.050\sigma_m$. In other words, there is no correction for lattice strain, which we show later to be a reasonable approximation.

Cuts through the (h, h, l) plane (which is perpendicular to the stress axis) under different applied stresses σ are shown in Fig. 2(a–e). At $\sigma = 0.050\sigma_m$, reflec-

tions from all three domain types are present. The reflections from the (100) and (010) domains are shifted rightward relative to those from the (110) domains by $\Delta q = 0.0006 \pm 0.0003$ r.l.u. Such an offset can also be seen in the data of nominally unstressed PdCrO₂ in Fig. 1(b), from Ref. [21], where $\Delta q = 0.0011 \pm 0.0003$ r.l.u.

As stress is applied the (110) reflections fade and disappear, which is in agreement with previous results [21]: in-plane uniaxial compression favors domains whose spin planes are more perpendicular to the stress axis. The (100) and (010) reflections shift further rightward. As $|\sigma|$ becomes large the reflections also become streaked, which is most likely a consequence of strain inhomogeneity. Strain homogeneity should also make the nuclear Bragg peaks streaked, but we find that q shifts rapidly with applied strain, so that streaking is far more pronounced in the magnetic peaks. q_1 , the location of the $l = 1$ reflection, versus applied stress σ is plotted in Fig. 2(k). Within resolution, the dependence is linear, and no locking to the commensurate value $1/3$ is resolved. Between $\sigma = 0$ and -0.4 GPa, q_1 shifts by 5%. For a Young's modulus of ~ 100 GPa, the longitudinal strain under $\sigma = -0.4$ GPa would be around -0.4% , and the Poisson's ratio expansion in the scattering plane perhaps half of this, or $+0.2\%$. In other words, the stress-driven shift in q_1 exceeds plausible strain in the sample by an order of magnitude, and we are justified in not correcting the indexing for lattice strain.

Because the spin planes of the (100) and (010) domains are neither aligned with nor perpendicular to the stress axis, there is no symmetry requirement for the reflections from these domains to have $h = k$; referring to Fig. 1(e), we do not require $\alpha = \beta$. In the Appendix cuts through the (h, k, l) plane are shown, which show that h and k of the reflections nevertheless remain approximately equal as stress is applied.

The fact that Δq is non-zero at the smallest applied stress, and also in the nominally unstressed sample shown in Fig. 1(b), indicates that the magnetic order is incommensurate even at very low applied stress, with an incommensuration period of around 1000 lattice spacings. To resolve such long-period incommensuration, it is useful to be able to compare reflections from different domains in this way, because it means that we do not rely solely on the global indexing of the reflections. A nonzero Δq was visible in the data of Ref. [21], but was not commented upon: the observation that Δq grows under stress gives confidence that it is a real feature of the data.

The paths traced by the $l = 1$ and $l = 2$ reflections in the (h, h, l) plane as stress is applied are shown in Fig. 2(l). It is apparent that as stress is applied the magnetism also becomes incommensurate along the c axis. The reflection that was at $l = 1$ shifts initially to an incommensurate position at $l < 1$, and then reverses direction to $l > 1$ as $|\sigma|$ increases further. The $l = 2$ reflection follows an opposite stress dependence, shifting initially

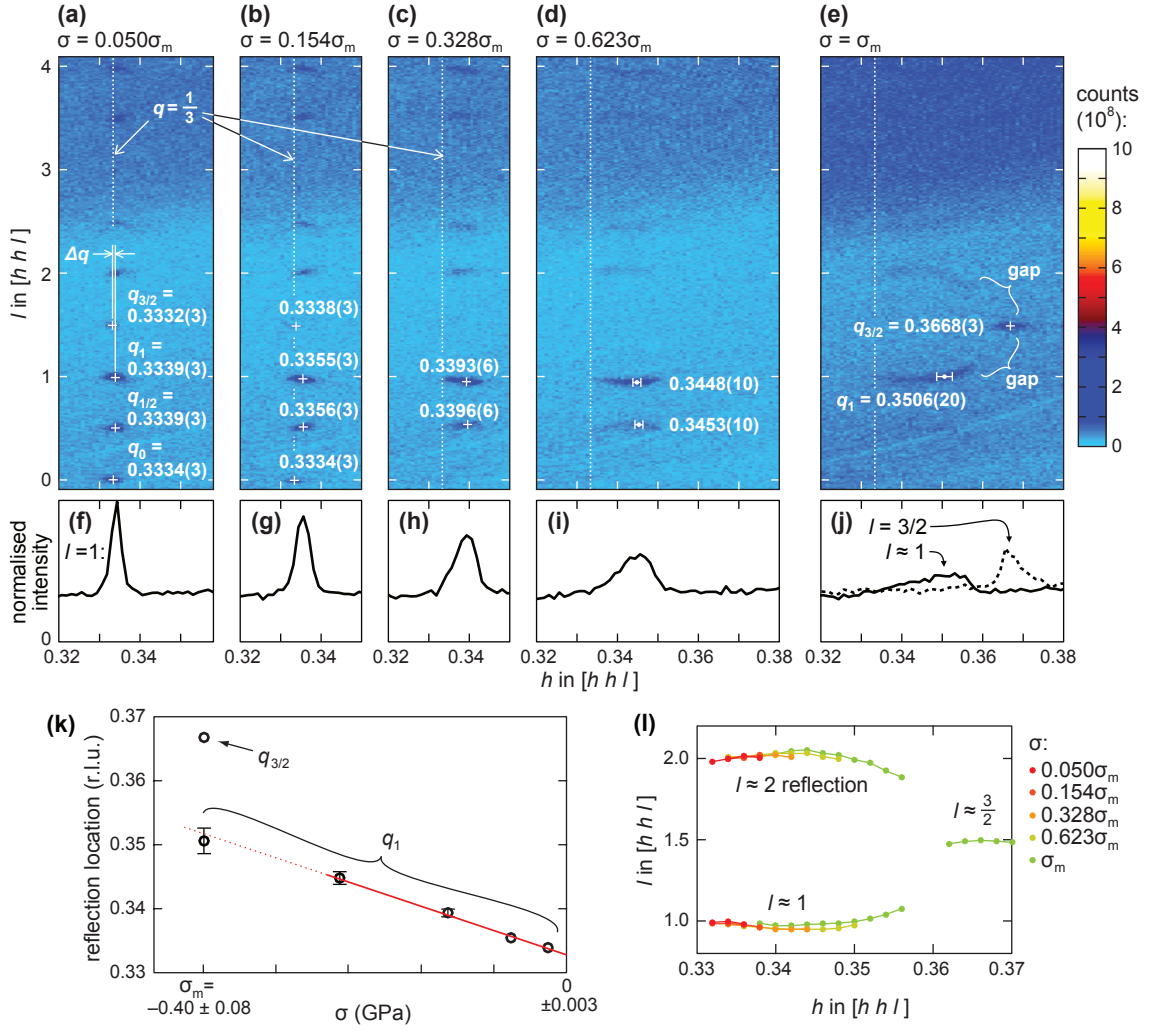


FIG. 2. Neutron scattering results, at 10 K. (a–e) Cuts through the (h, h, l) plane at different uniaxial stresses σ applied along the $[\bar{1}\bar{1}0]$ direction. The largest stress applied was $\sigma_m = -0.40 \pm 0.08$ GPa. The centres of selected reflections are indicated. The peak shape varies with stress and is not straightforward to fit with a single model, so the centres and error bars are judged by eye. These errors exclude any global error in the indexing. All reflections are indexed according to the Bragg reflections at $\sigma = 0.050\sigma_m$ GPa. (f–j) Cuts through the $l \approx 1$ reflections and, in panel (j), the $l = \frac{3}{2}$ reflection. In these plots, intensity is integrated over ± 0.15 in l and ± 0.03 in $[h, -h, l]$. (k) Location q_1 of the $l \approx 1$ reflection along the $h = k$ axis versus applied stress. The line is a fit through the first four points; the dotted portion is an extrapolation. (l) Paths traced by the $l \approx 1$, $l \approx 2$, and, at $\sigma = \sigma_m$, $l \approx \frac{3}{2}$ reflections in the (h, h, l) plane as stress is applied. The points mark the intensity maxima along cuts along the l axis.

to $l > 2$, then $l < 2$.

We do not detect any scattering intensity for h between 0.357 and 0.367, where there is then a strong reflection at $l = \frac{3}{2}$. This gap is highlighted in Fig. 2(e). We interpret these data as showing a first-order transition in the magnetic structure. In this interpretation, the reflections at $l \approx 1$ and $l \approx 2$ in the small- $|\sigma|$ structure shift continuously to larger q as $|\sigma|$ is increased, eventually reaching $q = 0.357$. But magnetic order is unstable for $0.357 < q < 0.367$. The low- and high-stress phases can coexist in equilibrium due to strain inhomogeneity. The cuts shown in Fig. 2(j) support this interpretation: the $l \approx 1$ reflection has a tail extending to $h < 0.357$, and the

$l = \frac{3}{2}$ has a tail extending to $h > 0.367$, but scattering intensity is cut off sharply between these two values.

The reflection $(0.367, 0.367, \frac{3}{2})$ is not accompanied by reflections at $l = 0$ and $l = 3$, showing that in the high- $|\sigma|$ phase the interlayer correlation is strictly antiferromagnetic. Also, from the fact that the high- $|\sigma|$ reflection is at $l = \frac{3}{2}$, it appears that strong compression along $[\bar{1}\bar{1}0]$ favors (110) domains, whereas weak compression favored (100) and (010) domains. The way that the reflections at $l \approx 1$ and $l \approx 2$ curve inwards towards $l = \frac{3}{2}$ as $|\sigma|$ increases suggests a rotation of the spin planes of the (100) and (010) domains towards the (110) plane as stress is applied. However, the data here are not sufficient for ac-

curate refinement of the magnetic structure under stress.

RESULTS: RESISTIVITY

We now show that this transition in interlayer ordering has an observable effect on in-plane resistivity. For resistivity measurements, a stress cell was used that had a sensor of the displacement but not the force applied to the sample, so strain rather than stress is the measured control variable. The applied strain is taken as the applied displacement divided by the exposed sample length, and then multiplied by a factor of 0.8 as an estimate for the loss due to elastic deformation of the epoxy.

Strain is applied along the length of the samples, and resistivity is measured along the same axis. Two samples were measured, labelled A and B. Some data on sample A were also shown in Ref. [21], where it was labeled Sample 1. In Fig. 3(a-b), we show the resistance versus $\varepsilon_{\bar{1}10}$ for sample A at temperatures up to 20 K. (Resistance rather than resistivity is shown because a contact to the sample broke — this sample was small — and so an unconventional contact configuration was used.) For temperatures below ~ 8 K, the dominant feature in the data is a first-order transition that was identified in Ref. [21] as reorientation of domains as the applied stress switches between compressive and tensile, and we therefore fix the neutral strain point $\varepsilon_{\bar{1}10} = 0$ at the centre of this transition.

For temperatures below ~ 8 K, a feature is also discernible at $\varepsilon_{\bar{1}10} \approx -3.5 \cdot 10^{-3}$. In the zero-field data from sample A it is subtle, but under a field it becomes much more prominent: see the data from sample B in Fig. 3(c). It also becomes clear that it is a first-order transition: there is definite hysteresis at 3 K, that mostly closes by 10 K. This is almost certainly the transition in interlayer ordering that is seen in the neutron data. In the neutron data, the transition occurs at a stress of ~ -0.4 GPa, and if this is equated with the transition strain $\varepsilon_{\bar{1}10} = -3.5 \cdot 10^{-3}$ seen in resistivity a Young's modulus of ~ 100 GPa is implied, which is a typical value for inorganic solids.

Resistivity data also show that strain has a nontrivial effect on the Néel transition. $R(T)$ of sample A at $T \sim T_N$ and at various fixed strains is shown in Fig. 4(a). At small applied strains, the Néel transition is apparent as a sharp drop in resistivity. Although no hysteresis was resolved, the step-like nature of the transition strongly suggests that it is first-order. As the sample is compressed, there is initially little change in this feature, but then it fades away. Under strong compression, a much broader feature is apparent in the data: a broad maximum in the slope dR/dT , indicated by the red arrow in Fig. 4(a) for the largest applied compression. Identifying this feature as the Néel transition, in Fig. 4(c) we show T_N versus strain, with the data points coloured by a measure of transition width. The crossover from

a first-order to a broad transition is associated with a change in the stress dependence of T_N : from a concave-downward, parabolic dependence to a steep linear dependence. Under tensile stress, the Néel transition began to broaden, suggesting that it would evolve similarly under strong tensile strain as under strong compressive strain. However, the sample then fractured as we attempted to tension it further.

DISCUSSION

We begin our Discussion with consideration of the rate of change of the magnetic structure with strain. The fact that q increases with compression along $[\bar{1}10]$ means that the magnetic lattice, like the real-space lattice, is tuned towards a square net: referring to Fig. 1(e), J_3 shrinks relative to J_1 and J_2 . The largest stress we achieve, $\sigma_m = -0.4$ GPa, is modest. If the Young's modulus is ~ 100 GPa, bonds along the stress axis would be compressed by $\sim 0.4\%$, and bonds perpendicular to the stress axis stretched by $\sim 0.2\%$, yielding a bond length anisotropy of $\sim 0.6\%$. The induced magnetic anisotropy appears to be much larger than this. At $\sigma = -0.4$ GPa, $q = 0.367$ for portions of the sample in the high- $|\sigma|$ state and up to 0.357 for portions in the low- $|\sigma|$ state. If interactions beyond nearest-neighbor are neglected, and J_1 and J_2 are taken to be equal, then $h = 0.367$ is obtained for $J_3/J_1 = 0.746$, and 0.357 for $J_3/J_1 = 0.803$ [3, 4]—the stress-induced anisotropy in nearest-neighbor interactions is about forty times the bond length anisotropy. Higher-order interactions will alter these values, but the point is that magnetic anisotropy grows very rapidly and so very substantial tuning of the magnetic structure is technically possible. For classical spins, spiral order is expected to undergo transition to linear antiferromagnetism at $J_3/J_1 = 0.5$ [4], and quantum corrections are predicted to shift this transition to higher J_3/J_1 [9, 10]. Extrapolation from the data here suggests that this transition should occur at $\sigma \sim -1$ GPa, which is an achievable stress [31].

We did not reach such strong compression here, however, and the observed first-order transition, the change in interlayer ordering, was unexpected. It suggests that interlayer ordering reflects a balance of interactions and so is somewhat delicate, an idea supported by the fact that other delafossite compounds with CrO_2 layers have different interlayer orderings: in LiCrO_2 , the helicity alternates from layer to layer [32], as in unstressed PdCrO_2 , but in CuCrO_2 and AgCrO_2 the interlayer correlation is ferromagnetic [24, 33, 34], while, as reported above, the interlayer ordering in PdCrO_2 under in-plane uniaxial stress is antiferromagnetic.

We discuss whether the magnetism of unstressed PdCrO_2 could be incommensurate. Unstressed AgCrO_2 and CuCrO_2 are both incommensurate, with $q = 0.327$

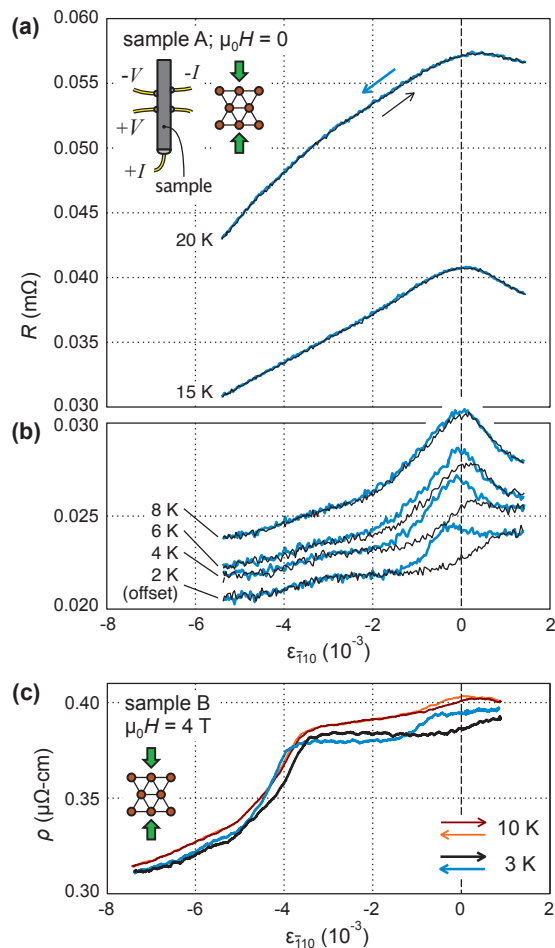


FIG. 3. (a-b) Resistance R versus strain $\varepsilon_{\bar{1}10}$ for sample A at various temperatures. Note the unconventional contact configuration, illustrated in the upper panel, due to a broken electrical contact. Data at 2 K are offset for clarity. (c) Resistivity under an applied field along the c axis $\mu_0 H = 4$ T for sample B, at 3 and 10 K. The first-order nature of the transition at $\varepsilon_{\bar{1}10} \approx -3.5 \cdot 10^{-3}$ is more apparent here than under zero field, in panel (a).

for the former and 0.329 for the latter [24, 34, 35]. q in unstressed PdCrO₂ appears to be much closer to $\frac{1}{3}$ than in these materials. The spontaneous rotational symmetry breaking in unstressed PdCrO₂ will have a lattice distortion associated with it, and it is possible that this distortion itself is sufficient to make the order incommensurate. Due to the possibility of residual thermal stresses on the MPa level, both here and in [21], we cannot definitively resolve whether the magnetic order would be incommensurate under truly zero stress. Doing so could be a subtle measurement challenge: with, for example, tetragonal to orthorhombic lattice distortions, a configuration of twin boundaries, parallel lines, is possible that allows each domain to fully relax elastically, but with three domain types such an arrangement of domain walls is not possible. Therefore, for measurement under truly zero stress, the sample would need to be polarised into a single domain.

Regardless of whether or not the magnetic order of un-

stressed PdCrO₂ is commensurate, the fact that the incommensuration period can reach 1000 lattice spacings shows that the net spin-lattice coupling in PdCrO₂ is extraordinarily weak. It may be weak enough that classical dipole-dipole interactions determine the orientation of the spin plane [36]. The spins in PdCrO₂ appear to be almost perfect Heisenberg spins, which places PdCrO₂ in an interesting regime for study of the thermodynamics of magnetic ordering.

We conclude our Discussion with some notes on the effect of strain on the Néel transition, which provides hints of interesting dynamics in the formation of magnetic order. As shown in Fig. 4(c), the first-order transition at T_N extends out to $|\varepsilon_{\bar{1}10}| \sim 3 \cdot 10^{-3}$. The transition might be driven first-order by fluctuations: fluctuations are expected to drive rotational-symmetry-breaking transitions first-order when the orientation is selected, as in PdCrO₂, from among three or more equivalent options [37, 38]. The strain range over which the transition is first-order

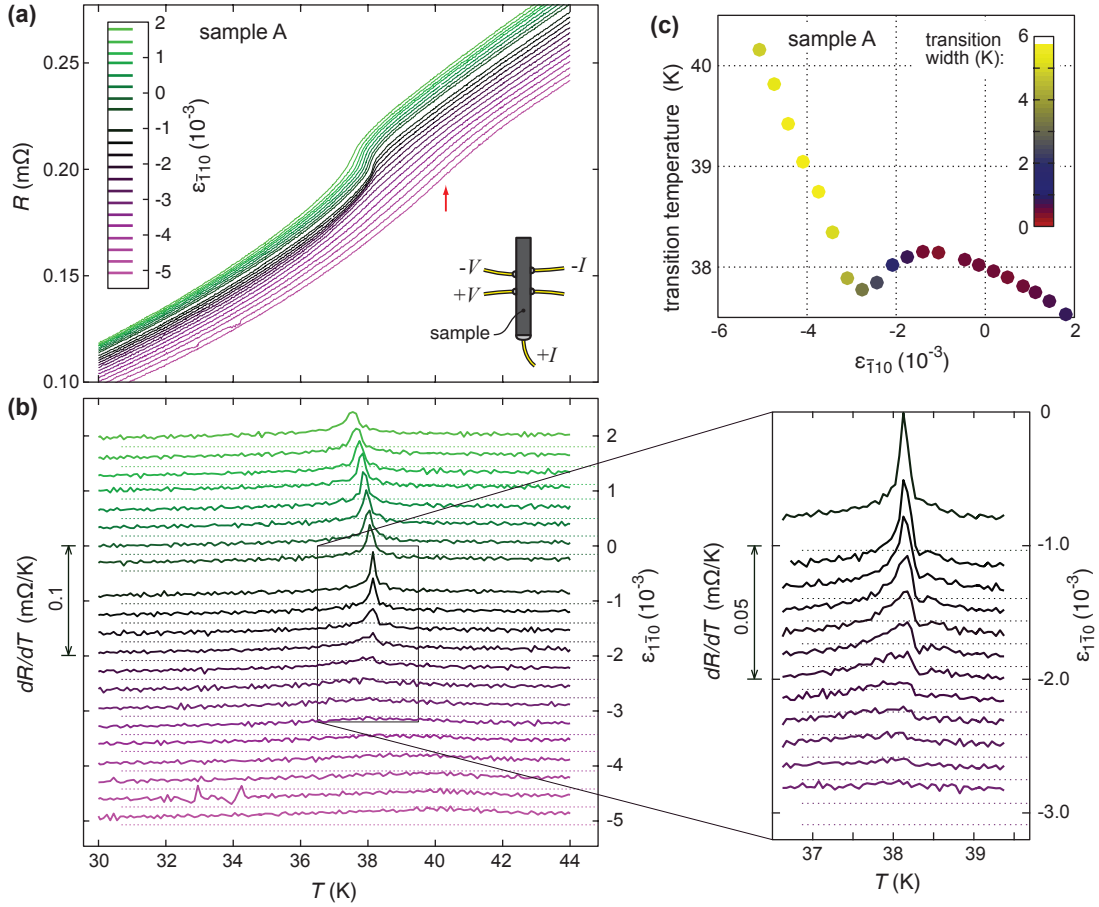


FIG. 4. (a) $R(T)$ of sample A at various strains ϵ_{110} . For small $|\epsilon_{110}|$, T_N is clearly discernible in the data. At larger $|\epsilon_{110}|$, the transitions broadens dramatically; at the maximum compression reached, $\epsilon_{110} \approx -5 \cdot 10^{-3}$, the transition is visible as a broad maximum in the slope dR/dT , indicated by the red arrow. (b) dR/dT at various strains. The dotted lines show the applied strain, indicated on the right-hand axis. (c) Transition temperature, identified as the temperature where $d^2R/dT^2 = 0$, versus ϵ_{110} . The symbol color indicates the width of the transition, taken as $[(1/R) \times |d^3R/dT^3|]^{-1/3}$ at the transition.

does not correspond to fluctuations at $T < T_N$: the domain reorientation transition at $\epsilon = 0$ has been found to be sharp for temperatures below, and right up to, T_N [21]. It may therefore correspond to the strain required to polarise the fluctuations at $T \gtrsim T_N$. In the mean field, the linear dependence of T_N on uniaxial stress observed for $|\epsilon_{110}| \gtrsim 3 \cdot 10^{-3}$ is the expected form for transition into a uniaxial order. PdCrO_2 may therefore provide an interesting, and very well-controlled, test case for study of the thermodynamic effect of fluctuations on ordering processes, which motivates further study of the transition at T_N .

ACKNOWLEDGEMENTS

We thank C. Broholm, C. M. Lee, A. Little, T. Oka, J. W. Orenstein, C. Timm, and M. Vojta for useful discussions. Experiments at the ISIS Pulsed Neutron and Muon Source were supported by a beam time alloca-

tion from the Science and Technology Facilities Council under Expt. No. RB1820290. Financial support from the Deutsche Forschungsgemeinschaft through SFB 1143 (Project ID 247310070) and the Max Planck Society is gratefully acknowledged. RW acknowledges funding and support from the Engineering and Physical Sciences Research Council (EPSRC) Centre for Doctoral Training in Condensed Matter Physics (CDT-CMP), Grant No. EP/L015544/1.

APPENDIX

Cuts in the $h, k, l = 1$ plane

In Fig. 5, we show cuts through the $l \approx 1$ reflection of Sample 1 in the h, k plane. At the smallest applied stress, in panel (a), the reflection lies close to the commensurate position $[\frac{1}{3}, \frac{1}{3}, l]$. As stress is applied, it moves outward to larger h and k . It appears not to follow the $h = k$ line

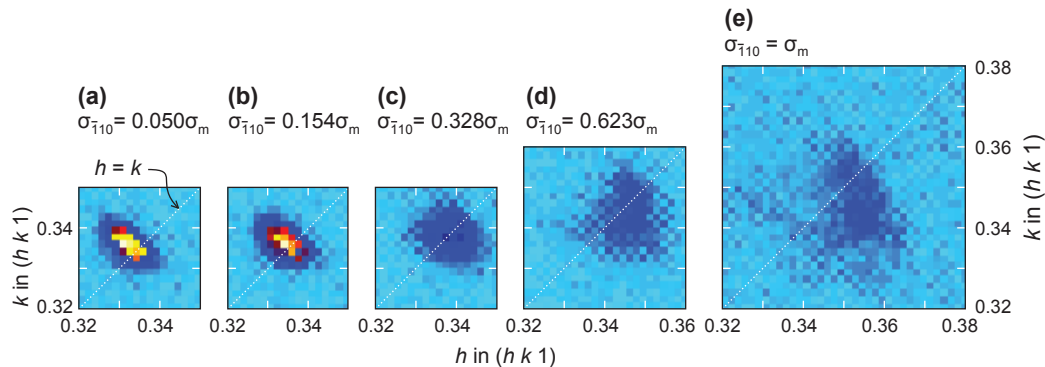


FIG. 5. Cuts through the $l \approx 1$ reflection in the $(h, k, l = 1)$.

precisely, though remains close enough that, within the resolution of these measurements, the cuts through the (h, h, l) plane in Fig. 2(a–e) give an accurate view of the evolution of the magnetic structure with stress.

Error on the stress calibration for neutron measurements

In the stress cell employed for neutron scattering, a mechanical contact can be opened between the piezoelectric actuators and the sample in order to bring the force applied to the sample to nearly zero. However, the device incorporates a series of flexures, described in Ref. [29], and the spring constant of these flexures, in combination with the differential thermal contraction between the sample and titanium, from which the sample holder is fabricated, can still result in a residual stress on the sample. The total flexure spring constant is $\approx 0.3 \text{ N}/\mu\text{m}$. A thermal contraction of 0.75% between room and cryogenic temperatures has been measured for PdCrO_2 [22], but this is extremely large; CuCrO_2 contracts by 0.25% between 300 and 10 K [35]. Ti contracts by 0.15%, so we estimate a differential thermal contraction between PdCrO_2 and Ti of $\sim 0.1\%$, and an effective sample length over which this differential operates of $\sim 2 \text{ mm}$. The force on the sample would then be of order $2 \mu\text{m} \times 0.3 \text{ N}/\mu\text{m} \sim 0.6 \text{ N}$, for a stress of $\sim 3 \text{ MPa}$.

The strain gauges on the sample holder were calibrated after the neutron scattering measurement as described in Ref. [29]. However, the response from the gauges was roughly half the expected value, based on finite element analysis of the deformation of the holder under applied stress. We therefore assign a relatively large error, $\pm 20\%$, to σ_m .

- antiferromagnets,” *Phys. Rev. B* **83**, 184401 (2011).
- [2] M. Poienar, F. Damay, C. Martin, J. Robert, and S. Petit, “Spin dynamics in the geometrically frustrated multiferroic CuCrO_2 ,” *Phys. Rev. B* **81**, 104411 (2010).
- [3] J. Villain, “La structure des substances magnetiques,” *J. Phys. Chem. Solids* **11**, 303 (1959).
- [4] A. Yoshimori, “A new type of antiferromagnetic structure in the rutile type crystal,” *J. Phys. Soc. Japan* **14**, 807 (1959).
- [5] P. Manuel, L. C. Chapon, I. S. Todorov, D. Y. Chung, J.-P. Castellan, S. Rosenkranz, R. Osborn, P. Toledano, and M. G. Kanatzidis, “Incommensurate spin-density wave and magnetic lock-in transition in CaFe_4As_3 ,” *Phys. Rev. B* **81**, 184402 (2010).
- [6] Y. Nambu, L. L. Zhao, E. Morosan, K. Kim, G. Kotliar, P. Zajdel, M. A. Green, W. Ratcliff, J. A. Rodriguez-Rivera, and C. Broholm, “Incommensurate magnetism in FeAs strips: neutron scattering from CaFe_4As_3 ,” *Phys. Rev. Lett.* **106**, 037201 (2011).
- [7] D. K. Pratt, M. G. Kim, A. Kreyssig, Y. B. Lee, G. S. Tucker, A. Thaler, W. Tian, J. L. Zarestky, S. L. Bud’ko, P. C. Canfield, B. N. Harmon, A. I. Goldman, and R. J. McQueeney, “Incommensurate spin-density wave order in electron-doped BaFe_2As_2 superconductors,” *Phys. Rev. Lett.* **106**, 257001 (2011).
- [8] E. Fawcett, H. L. Alberts, V. Y. Galkin, D. R. Noakes, and J. V. Yakhmi, “Spin-density-wave antiferromagnetism in chromium alloys,” *Rev. Mod. Phys.* **66**, 25 (1994).
- [9] J. Merino, R. H. McKenzie, J. B. Marston, and C. H. Chung, “The Heisenberg antiferromagnet on an anisotropic triangular lattice: linear spin-wave theory,” *J. Phys.: Condens. Matter* **11**, 2965 (1999).
- [10] W. H. Zheng, R. H. McKenzie, and R. R. P. Singh, “Phase diagram for a class of spin- $\frac{1}{2}$ Heisenberg models interpolating between the square-lattice, the triangular-lattice, and the linear-chain limits,” *Phys. Rev. B* **59**, 14367 (1999).
- [11] A. P. Mackenzie, “The properties of ultrapure delafossite metals,” *Rep. Prog. Physics* **80**, 032501 (2017).
- [12] V. Sunko, F. Mazzola, S. Kitamura, S. Khim, P. Kushwaha, O. J. Clark, M. D. Watson, I. Marković, D. Biswas, L. Pourovskii, T. K. Kim, T.-L. Lee, P. K. Thakur, H. Rosner, A. Georges, R. Moessner, T. Oka, A. P. Mackenzie, and P. D. C. King, “Probing spin correlations using angle-resolved photoemission in a coupled metal-

[1] L. Messio, C. Lhullier, and G. Misguich, “Lattice symmetries and regular magnetic orders in classical frustrated

- lic/Mott insulator system,” *Sci. Advances* **6**, eaaz0611 (2020).
- [13] F. Lechermann, “Hidden Mott insulator in metallic PdCrO₂,” *Phys. Rev. Mat.* **2**, 085004 (2018).
- [14] H. Takatsu, H. Yoshizawa, S. Yonezawa, and Y. Maeno, “Critical behavior of the metallic triangular-lattice Heisenberg antiferromagnet PdCrO₂,” *Phys. Rev. B* **79**, 144424 (2009).
- [15] H. Takatsu, S. Yonezawa, C. Michioka, K. Yoshimura, and Y. Maeno, “Anisotropy in the magnetization and resistivity of the metallic triangular-lattice magnet PdCrO₂,” *J. Phys.: Conf. Series* **200**, 012198 (2010).
- [16] C. W. Hicks, A. S. Gibbs, L. Zhao, P. Kushwaha, H. Borrmann, A. P. Mackenzie, H. Takatsu, S. Yonezawa, Y. Maeno, and E. A. Yelland, “Quantum oscillations and magnetic reconstruction in the delafossite PdCrOa₂,” *Phys. Rev. B* **92**, 014425 (2015).
- [17] R. Daou, R. Frésard, S. Hébert, and A. Maignan, “Impact of short-range order on transport properties of the two-dimensional metal PdCrO₂,” *Phys. Rev. B* **92**, 245115 (2015).
- [18] S. Arsenijević, J. M. Ok, P. Robinson, S. Ghannadzadeh, M. I. Katsnelson, J. S. Kim, and N. E. Hussey, “Anomalous Magnetothermopower in a Metallic Frustrated Antiferromagnet,” *Phys. Rev. Lett.* **116**, 087202 (2016).
- [19] D. Billington, D. Ernsting, T. E. Millichamp, C. Lester, S. B. Dugdale, D. Kersh, J. A. Duffy, S. R. Giblin, J. W. Taylor, P. Manuel, D. D. Khalyavin, and H. Takatsu, “Magnetic frustration, short-range correlations and the role of the paramagnetic Fermi surface of PdCrO₂,” *Sci. Reports* **5**, 12428 (2015).
- [20] S. Ghannadzadeh, S. Licciardello, S. Arsenijević, P. Robinson, H. Takatsu, M. I. Katsnelson, and N. E. Hussey, “Simultaneous loss of interlayer coherence and long-range magnetism in quasi-two-dimensional PdCrO₂,” *Nat. Commun.* **8**, 15001 (2017).
- [21] D. Sun, D. A. Sokolov, J. M. Bartlett, J. Sannigrahi, S. Khim, P. Kushwaha, D. D. Khalyavin, P. Manuel, A. S. Gibbs, H. Takagi, A. P. Mackenzie, and C. W. Hicks, “Magnetic frustration and spontaneous rotational symmetry breaking in PdCrO₂,” *Phys. Rev. B* **100**, 094414 (2019).
- [22] H. Takatsu, G. Nénert, H. Kadowaki, H. Yoshizawa, M. Enderle, S. Yonezawa, Y. Maeno, J. Kim, N. Tsuji, M. Takata, Y. Zhao, M. Green, and C. Broholm, “Magnetic structure of the conductive triangular-lattice antiferromagnet PdCrO₂,” *Phys. Rev. B* **89**, 104408 (2014).
- [23] E. V. Komleva, V. Y. Irkhin, I. V. Solovyev, M. I. Katsnelson, and S. V. Streltsov, “Unconventional magnetism and electronic state in the frustrated layered system PdCrO₂,” *Phys. Rev. Lett.* **102**, 174438 (2020).
- [24] M. Frontzek, G. Ehlers, A. Podlesnyak, H. Cao, M. Matsuda, O. Zaharko, N. Aliouane, and S. V. Barilo, S. Shiryayev, “Magnetic structure of CuCrO₂: a single crystal neutron diffraction study,” *J. Phys.: Condens. Matter* **24**, 016004 (2012).
- [25] M. Soda, K. Kimura, T. Kimura, and K. Hirota, “Domain rearrangement and spin-spiral-plane flop as sources of magnetoelectric effects in delafossite CuCrO₂,” *Phys. Rev. B* **81**, 100406 (2010).
- [26] H. Takatsu, S. Yonezawa, S. Fujimoto, and Y. Maeno, “Unconventional Anomalous Hall Effect in the Metallic Triangular-Lattice Magnet PdCrO₂,” *Phys. Rev. Lett.* **105**, 137201 (2010).
- [27] M. Akaike, Y. Nii, H. Masuda, and Y. Onose, “Nonreciprocal electronic transport in PdCrO₂: Implication of spatial inversion symmetry breaking,” *Phys. Rev. B* **103**, 184428 (2021).
- [28] J. M. Ok, Y. J. Jo, K. Kim, T. Shishidou, E. S. Choi, H.-J. Noh, T. Oguchi, B. I. Min, and J. S. Kim, “Quantum Oscillations of the Metallic Triangular-Lattice Antiferromagnet PdCrO₂,” *Phys. Rev. Lett.* **111**, 176405 (2013).
- [29] S. Ghosh, F. Brückner, A. Nikitin, V. Grinenko, M. Elenker, A. P. Mackenzie, H. Luetkens, H.-H. Klauss, and C. W. Hicks, “Piezoelectric-driven uniaxial pressure cell for muon spin relaxation and neutron scattering experiments,” *Rev. Sci. Instr.* **91**, 103902 (2020).
- [30] L. C. Chapon, P. Manuel, P. G. Radaelli, C. Benson, L. Perrott, S. Ansell, N. J. Rhodes, D. Raspino, D. Duxbury, E. Spill, and J. Norris, “Wish: The new powder and single crystal magnetic diffractometer on the second target station,” *Neutron News* **22**, 22 (2011).
- [31] M. E. Barber, A. Steppke, A. P. Mackenzie, and C. W. Hicks, “Piezoelectric-based uniaxial pressure cell with integrated force and displacement sensors,” *Rev. Sci. Instr.* **90**, 023904 (2019).
- [32] H. Kadowaki, H. Takei, and K. Motoya, “Double-*Q* 120° structure in the Heisenberg antiferromagnet on rhombohedrally stacked triangular lattice LiCrO₂,” *J. Phys.: Condens. Matter* **7**, 6869 (1995).
- [33] H. Kadowaki, H. Kikuchi, and Y. Ajiro, “Neutron powder diffraction study of the two-dimensional triangular lattice antiferromagnet CuCrO₂,” *J. Phys.: Condens. Matter* **2**, 4485 (1990).
- [34] Y. Oohara, S. Mitsuda, H. Yoshizawa, N. Yaguchi, H. Kuriyama, T. Asano, and M. Mekata, “Magnetic phase transition in AgCrO₂,” *J. Phys. Soc. Japan* **63**, 847 (1994).
- [35] M. Poienar, F. Damay, C. Martin, V. Hardy, A. Maignan, and G. André, “Structural and magnetic properties of CuCr_{1-x}Mg_xO₂ by neutron powder diffraction,” *Phys. Rev. B* **79**, 014412 (2009).
- [36] M. D. Le, S. Jeon, A. I. Kolesnikov, D. J. Voneshen, A. S. Gibbs, J. S. Kim, J. Jeong, H.-J. Noh, C. Park, J. Yu, T. G. Perring, and J.-G. Park, “Magnetic interactions in PdCrO₂ and their effects on its magnetic structure,” *Phys. Rev. B* **98**, 024429 (2018).
- [37] M. Hecker and J. Schmalian, “Vestigial nematic order and superconductivity in the doped topological insulator Cu_xBi₂Se₃,” *npj Quant. Mater.* **3**, 26 (2018).
- [38] A. Little, C. Lee, C. John, S. Doyle, E. Maniv, N. L. Nair, W. Chen, D. Rees, J. W. F. Verderbos, R. M. Fernandes, J. G. Analytis, and J. Orenstein, “Three-state nematicity in the triangular lattice antiferromagnet Fe_{1/3}NbS₂,” *Nat. Mater.* **19**, 1062 (2020).